

Sphingosine Kinase Inhibition Enhances Dimerization of Calreticulin at the Cell Surface in Mitoxantrone-Induced Immunogenic Cell Death.

Asvelt J. Nduwumwami, Jeremy A. Hengst and Jong K. Yun

Department of Pharmacology, Pennsylvania State University College of Medicine, 500
University Drive, Hershey, PA USA 17033.

To whom correspondence should be addressed:

Jong K. Yun

Department of Pharmacology

Pennsylvania State University College of Medicine

500 University Drive

Hershey, PA 17033-0850

Phone: 717-531-1508

Fax: 717-531-5013

Email: jky1@psu.edu

Running Title: Sphingosine kinase inhibitors enhance dimeric calreticulin

of Text Pages: 23

of Tables: 0

of Figures: 6

of References: 68

of words, Abstract: 239

of words, Introduction: 903

of words, Discussion: 1300

Non-standard Abbreviations:

ICD - immunogenic cell death

DAMPs - danger-associated molecular patterns

DCs - dendritic cells

MTX - mitoxantrone

PERK - protein kinase RNA-like endoplasmic reticulum kinase

eIF2 α - eukaryotic initiating factor 2 α

CRT - calreticulin

ectoCRT – cell surface exposed CRT

Cer - ceramide

S1P - sphingosine-1-phosphate

Sph - sphingosine

dhSph - dihydroSph

CerS1-6 - ceramide synthases 1-6

SphKs - sphingosine kinases

SKIs - SphK inhibitors

SRB - Sulforhodamine B

PE - phycoerythrin

β-ME - β-mercaptoethanol

Recommended Section Assignment:

Chemotherapy, Antibiotics, and Gene Therapy

ABSTRACT

Agents that induce immunogenic cell death (ICD) alter the cellular localization of calreticulin (CRT) causing it to become cell surface exposed within the plasma membrane lipid raft microdomain (ectoCRT) where it serves as a damage associated molecular pattern that elicits an antitumor immune response. We have identified the sphingolipid metabolic pathway as an integral component of the process of ectoCRT exposure. Inhibition of the sphingosine kinases (SphKs) enhances mitoxantrone-induced production of hallmarks of ICD including ectoCRT production, with an absolute mean difference of 40 MFI (95% CI: 19 to 62; $P=0.0014$) and 1.3 fold increase of ATP secretion with an absolute mean difference of 87 RLU (95% CI: 55 to 120; $P<0.0001$). Mechanistically, sphingosine kinase inhibition increases mitoxantrone-induced accumulation of ceramide species including C16:0 ceramide 2.8 fold with an absolute mean difference of 1.390 pmoles/nmoles Pi (95% CI: 0.798 to 1.983; $P=0.0023$). We further examined the localization of ectoCRT to the lipid raft microdomain and demonstrate that ectoCRT forms disulfide bridged dimers. Together, our findings suggest that ceramide accumulation impinges on the homeostatic function of the endoplasmic reticulum to induce ectoCRT exposure and that structural alterations of ectoCRT may underlie its immunogenicity. Our findings further suggest that inhibition of the SphKs may represent a means to enhance the therapeutic immunogenic efficacy of ICD-inducing agents while reducing overt toxicity/immunosuppressive effects by allowing for the modification of dosing regimens or directly lowering the dosages of ICD-inducing agents employed in therapeutic regimens.

SIGNIFICANCE STATEMENT

This study demonstrates that inhibition of sphingosine kinase enhances the mitoxantrone-induced cell surface exposure of a dimeric form of the normally endoplasmic reticulum resident chaperone calreticulin as part of the process of a unique form of regulated cell death termed immunogenic cell death. Importantly, inhibition of sphingosine kinase may represent a means to enhance the therapeutic efficacy of immunogenic cell death-inducing agents, such as mitoxantrone, while reducing their overt toxicity and immunosuppressive effects leading to better therapeutic outcomes for patients.

INTRODUCTION

The recent discovery of immunogenic cell death (ICD) has opened a new field of cancer therapeutics research at the frontier of immunology and cancer biology (Galluzzi et al., 2018; Marshall and Djamgoz, 2018). Through numerous studies, investigators have demonstrated that certain chemotherapeutic agents induce cancer cells to expose, or release, a cohort of normally intracellular proteins collectively termed danger-associated molecular patterns (DAMPs) to initiate an innate/adaptive immune response (Kepp et al., 2014). In contrast, chemotherapeutic agents that are unable induce ICD fail to promote DAMP release. These DAMPs act as “find-me” and “eat-me” signals to recruit/activate dendritic cells (DCs), “professional” antigen-presenting cells, to phagocytose cancer cells and drive the production of type I interferons (e.g. IFN γ) (Galluzzi et al., 2017). These DCs engulf the dying cancer cells and initiate an immune response by presenting captured antigens and priming the immune system to mount an attack on the tumor.

Certain chemotherapeutic agents such as the anthracycline, mitoxantrone (MTX), have been consistently shown to induce ICD in multiple cell types *in vitro* and *in vivo* (Galluzzi et al., 2015). Some of the events that lead to DAMP production have been delineated. MTX has been shown to act independently of its topoisomerase inhibitory activity to stimulate the protein kinase RNA-like endoplasmic reticulum kinase (PERK) arm of the unfolded protein response pathway (Obeid et al., 2007b; Panaretakis et al., 2009). PERK (eukaryotic initiating factor 2 kinase 3) subsequently phosphorylates eukaryotic initiating factor 2 α (eIF2 α) at Ser51 to inhibit cap-dependent protein translation. In fact, induction of eIF2 α phosphorylation has been reported to be absolutely required for production of DAMPs including cell surface exposure of the normally endoplasmic reticulum resident chaperone calreticulin (CRT) (Bezu et al., 2018). To date, however, the mechanism by which MTX induces cell surface expression of CRT remains unclear.

The sphingolipid metabolic pathway has previously been implicated in the mechanism of cell death induced by anthracyclines (Lucci et al., 1999a; Lucci et al., 1999b; Cuvillier et al., 2001). In particular, two predominant sphingolipids, ceramide (Cer) and sphingosine-1-phosphate (S1P) have been demonstrated to modulate the efficacy of the anthracycline, doxorubicin in multiple cancer types. Cer, a pro-apoptotic sphingolipid enhances cell death induced by doxorubicin (Grammatikos et al., 2007). Conversely, S1P functions as a pro-survival sphingolipid and has been shown to protect against doxorubicin-induced cell death and mediate intrinsic resistance to doxorubicin (Gucluler et al., 2011; Hazar-Rethinam et al., 2015; Ren and Su, 2020).

Sphingolipids are produced through the de novo synthesis pathway in the ER. As the penultimate product of de novo synthesis, Cer induces cell growth arrest or cell death by modulating multiple signaling pathways including the MAPK, and PI3K-AKT signaling pathways (Ohta et al., 1995; Sweeney et al., 1996; Sakakura et al., 1997; Shirahama et al., 1997; Qiu et al., 2006; Kim et al., 2008; Nica et al., 2008). To attenuate cell death, Cer can be further modified by the addition of glycosyl- or phosphocholine groups or hydrolyzed to produce sphingosine (Sph). Sph and dihydroSph (dhSph) can be recycled by the ceramide synthases (CerS1-6) back into Cer and dhCer, respectively (recycling pathway).

Alternately, Sph/dhSph can be phosphorylated by sphingosine kinases (SphKs) to produce anti-apoptotic/pro-survival S1P/dhS1P (Truman et al., 2014). Importantly, the SphKs control the fate of Sph within the cell (i.e. the “Sphingolipid Rheostat”). When activated, such as under stress conditions, the SphKs produce S1P, at the expense of Cer accumulation, to favor cell survival (Cuvillier et al., 1996). Conversely, SphK inhibitors (SKIs) blocks the production of

S1P/dhS1P and simultaneously increase the levels of Cer in cells through the recycling pathway.

Multiple lines of evidence indicate that Cer is linked to the intracellular processes that lead to ICD. For instance, doxorubicin and MTX, as well as photo-dynamic therapy, have all been shown to induce Cer accumulation (Nemoto et al., 2009; Rath et al., 2009; Gong et al., 2014; Korbelik et al., 2014; Wallington-Beddoe et al., 2017). Secondly, activation of the ceramide synthases and Cer accumulation have been shown to induce ER stress, which is involved in the cell surface exposure of CRT (Park et al., 2008a; Park et al., 2008b; Walker et al., 2009; Wang et al., 2017). Lastly, increasing the Cer content of lipid rafts causes clustering of lipid raft components involved in ICD including PERK, CD95, and the pro-apoptotic Bcl-2 proteins Bak and Bax (Park et al., 2008a; Park et al., 2008b; Panaretakis et al., 2009; Park et al., 2009; Siskind et al., 2010; Beverly et al., 2013). Importantly, we have previously demonstrated that SphK1 localizes to the PM lipid raft and mediates pro-survival signaling under stress conditions, such as serum deprivation, by attenuating the production of Cer (Hengst et al., 2009).

In this work, we set out to determine whether the sphingolipid metabolic pathway had a role in the production of cell surface exposed CRT. We demonstrate that SphK inhibition enhances MTX induced cell death and MTX induced Cer accumulation. Importantly, we demonstrate, for the first time, that SphK inhibition/Cer accumulation enhances cell surface exposure of CRT. Furthermore, we also demonstrate that the form of CRT generated by combined treatment with MTX and SKIs is almost exclusively a disulfide linked dimer that relocates to Cer-enriched lipid rafts. Together these findings show that the sphingolipid metabolic pathway modulates the effects of ICD inducers. Blocking SphK activity and promoting Cer accumulation alters CRT by promoting disulfide linkage dimer formation, a modification that

could potentially underlie the difference between immunogenic CRT and non-immunogenic CRT.

MATERIALS AND METHODS

Reagents and Antibodies

Cisplatin, Mitoxantrone, PF-543 and ABC294640 were all purchased from Selleckchem (Houston, TX). SK1-I was purchased from Enzo Life Sciences (Farmingdale, NY). Cisplatin and Mitoxantrone were freshly prepared in culture media prior to each experiment. PF-543 and ABC294640 were prepared in a DMSO vehicle. Anti-Calreticulin, anti-Cleaved Caspase 3, anti-Cleaved PARP, anti-caveolin-1, anti-Vinculin, anti-phospho eIF2 α Ser51 and total anti-eIF2 α antibodies were from Cell Signaling Technologies (Beverly, MA), anti-GAPDH antibodies were from Santa Cruz Biotechnologies (Dallas, TX).

Cell Lines and Culture Conditions

Human colorectal DLD-1 (CCL-221) and mouse colorectal CT-26 (CRL-2638) cells were obtained from ATCC, (Manassas, VA). Mouse colorectal MC-38 (ENH204-FP) cells were obtained from (Kerafast, Boston MA). All cells were cultured at 37°C in a humidified atmosphere of 5% CO₂ in Dulbecco's Modified Eagle Medium (DMEM) supplemented with 10% fetal bovine serum (FBS) and penicillin/streptomycin.

Detection of Cell Surface CRT

For treatment, cells were seeded at about 3×10^5 cells/well in six well plates in complete DMEM for 24h, then transferred to DMEM containing 5% FBS and penicillin/streptomycin in the presence of treatments for 48h. Cells were collected by trypsinization, followed by three washes

in PBS containing 2% FBS, stained with anti-calreticulin (D3E6) phycoerythrin (PE) conjugated antibody at 4°C for 1h, washed as above, and CRT was detected by Muse cell analyzer (SmartFlare detection settings described in results).

Sulforhodamine B Assay

Cells were treated with MTX and/or SKIs, at the concentrations indicated in the relevant figures, for 48h. Cell viability was measured using by Sulforhodamine B (SRB) staining (Vichai and Kirtikara, 2006). Briefly, culture media was aspirated and cell were fixed in ice cold 10% TCA at 4°C for 1h. Fixed cells were extensively washed in water and plates were allowed to dry. Cells were stained with 0.057% (wt/vol) SRB in 1% acetic acid for 30 min, washed extensively with 1% acetic acid and allowed to dry thoroughly. Dye was solubilized by the addition of 10 mM Tris base (pH 10.5) and absorbance was recorded at 510 nm in a microplate reader.

Sphingolipid Analysis

DLD-1 cells were treated with MTX (4 μ M) and/or PF-543 (5 μ M) for 48h. Individual cell samples were collected by trypsinization, pelleted and washed with PBS and flash frozen. Sphingolipidomic analysis was conducted by the Lipidomic Shared Resource Facility (Medical University of South Carolina, Charleston SC). Sphingolipid levels were expressed as pmoles of sphingolipid per nmole of inorganic phosphate (pmoles/nmole Pi).

Whole Cell Lysate Preparation

Total cell lysate was obtained by incubating treated and untreated DLD-1 cells in 1X RIPA (Cell Signaling Tech, Beverly MA), with phosphatase inhibitor cocktail and protease inhibitor tablets (Roche), for 30min at 4°C and followed by removal of cell debris by

centrifugation at 20,000 x g at 4°C. Protein concentrations were determined by BCA Assay (Pierce, Waltham MA).

Subcellular Fractionation

Triton X-100 soluble and insoluble total membrane fractions were isolated according to Hengst et al., (Hengst et al., 2009) with minor modifications. DLD-1 cells seeded and treated in 10 cm dishes were collected by trypsinization, and media separated by centrifugation at 500 x g for 5min at 4°C. Cells were washed once in PBS and flash frozen. After thawing, cells were resuspended in 1ml of 1X MBS (25mM MES, 150mM NaCl, pH 6.5) containing phosphatase inhibitor cocktail and a protease inhibitor tablet (Roche) and sonicated (3-15sec pulses 50% output). Nuclear debris and unlysed cells were removed from the post nuclear supernatant by centrifugation at 500 x g for 5min at 4°C and cytosolic fraction was isolated by centrifugation at 100,000 x g for 30min at 4°C. The total membrane proteins were resuspended in 500 µL of 1X MBS + 1% Triton X-100 containing phosphatase inhibitor cocktail and a protease inhibitor tablet, sonicated and left on ice for 30 min to solubilize. Triton X-100 soluble proteins were separated from Triton X-100 insoluble membranes by centrifugation at 100,000 x g for 30min at 4°C. The Triton X-100 insoluble fraction was resuspended in 1X RIPA containing phosphatase inhibitor cocktail and a protease inhibitor tablet followed by brief sonication, incubation on ice for 30min and centrifugation at 100,000xg for 30min at 4°C. Protein concentrations were determined by BCA Assay (Pierce, Waltham MA).

Immunoblot Analysis

Protein samples were separated on 4-12% NuPAGE gradient gels and transferred to PVDF membranes. Membranes were blocked with 5% milk in TBS-T followed by incubation in primary antibodies for 1h. After three 15min washes with TBS-T, membranes were incubated in

respective secondary antibodies and visualized on X-ray film using Super-Signal West Dura reagents (Pierce, Waltham MA).

ATP Assay

Extracellular release of ATP to the culture media was determined using the ENLITEN ATP Assay (Promega, Madison WI) according to the manufacturer's directions.

Statistical Analysis

SRB assays are reported as mean \pm SD. Flow cytometric data were either reported as raw mean fluorescent intensity \pm standard deviation or normalized to vehicle treated controls and the average fold-change was reported \pm standard deviation. ATP release assays were reported as raw relative light units \pm standard deviation. Statistical analysis of flow cytometric, ATP release and sphingolipidomic data were performed using one-way ANOVA followed by Tukey's multiple comparison test using GraphPad PRISM. Results are reported with 95% CI ranges determined by Tukey's test with p values.

RESULTS

Mitoxantrone induces ER stress and calreticulin exposure on the surface of colorectal cancer cells.

To investigate whether MTX was able to induce cell surface exposure of CRT, in human and murine colorectal cancer cell lines, we developed a simple, single-antibody, flow cytometry based assay employing the MUSE bench-top flow cytometer (Millipore, Burlington MA). Unlike typical flow-cytometry assays that use targeted primary antibodies and fluorescently-labeled secondary antibodies, we employed a phycoerythrin (PE)-conjugated anti-CRT antibody (clone D3E6; Cell Signaling Tech, Beverly MA) for staining of cell surface CRT. Using the SmartFlare detection settings on the MUSE flow-cytometer, CRT-PE was excited by green laser (532nm)

and PE excitation was detected by the yellow filter at (582nm). The primary advantage of a single fluorescently-labeled primary antibody detection system is that it decreases the likelihood of background staining arising from the secondary antibody. The major limitation of such a system is the reduced sensitivity due to the lack of signal amplification found in a two-antibody system.

The human CRC cell line, DLD-1, was treated with the known ICD-inducer MTX and an agent known to be deficient in ICD-induction, cisplatin, and the levels of cell surface CRT exposure were determined by flow cytometry. When compared to vehicle (DMSO) treated cells (average MFI 17.67) MTX treatment resulted in an approximately 2.5 fold increase in levels of CRT displayed on the cell surface (average MFI 46.40; 95% CI 16.64 to 40.82; $P=0.0008$). In contrast to MTX treatment, CRT levels in cisplatin treated cells did not differ from those observed in vehicle treated cells (Figure 1A). These results are consistent with published reports that cisplatin does not cause CRT to translocate to cell surface (Obeid et al., 2007b).

Multiple studies have implicated ER stress as a necessary component of the surface CRT translocation process (Obeid et al., 2007a; Panaretakis et al., 2009; Garg et al., 2012b; Wernitznig et al., 2019). To determine if MTX-induced CRT exposure correlated with its ability to induce ER stress in DLD-1 cells, we assessed phosphorylation levels of eIF2 α at serine 51 in whole cell lysates by western blot analysis. Our results show that MTX caused dose dependent induction of ER stress as indicated by phosphorylation at serine 51 of eIF2 α (Figure 1B).

Inhibition of the sphingosine kinases (SphKs) enhances MTX induced cell death.

MTX has been shown to induce production of DAMPs (e.g. cell surface expressed CRT, and secretion of ATP and high mobility group box 1; HMGB1) in enucleated cancer cells

indicating that the DNA damaging activity of MTX is not required for ICD induction (Obeid et al., 2007b). To examine the effects of altered sphingolipid metabolism, we first treated the mouse CRC cell line CT-26 (routinely used for ICD experiments (Kepp et al., 2014)) with multiple SphK inhibitors including, PF-543 (Schnute et al., 2012), ABC294640 (ABC) (French et al., 2010) and SK1-I (Paugh et al., 2008) for 48 hours and examined cell viability by sulforhodamine B (SRB) assays. As shown in Figure 2A, in the absence of MTX, none of the SKIs reduced cell viability, relative to vehicle controls, at the concentrations employed. In contrast, MTX reduced cell viability as low as 1 μ M when employed alone. At 1 μ M MTX, both doses of PF-543, and the highest dose of ABC and SK1-I (3.8 and 7.5 μ M, respectively) significantly decreased CT-26 cell viability relative to 1 μ M MTX alone ($P < 0.0006$ for 2.5 μ M PF-543 all other $P < 0.0001$). At doses of 2 and 4 μ M MTX, all three SKIs tested significantly enhanced the reduction of cell viability relative to MTX alone ($P < 0.0001$ at all concentrations).

We recently examined the isoform selectivity of multiple SKIs using the Cellular Thermal Shift Assay (CETSA), a whole cell assay of target engagement (Hengst et al., 2020). These studies revealed that at the concentrations commonly employed in the literature the SKIs tested, including PF-543 (SphK1-selective), ABC (SphK2-selective) and SK1-I (SphK1-selective), target engaged both SphK1 and SphK2. The concentrations of ABC and SK1-I, employed in Figure 2A, are below the concentrations we previously examined and we therefore cannot say for sure whether these agents target both SphK1 and SphK2. However, for PF-543, we determined the IC_{50} for target engagement of SphK2 to be approximately 2.5 μ M. Thus, it is possible that inhibition of both SphK1 and SphK2 is required to enhance the cytotoxic effects of MTX.

To better define the relative contribution of SphK1 and SphK2 inhibition to the enhancement of MTX cytotoxicity, we next examined the effects of lower concentrations of PF-543 and ABC and their combinations in human DLD-1 cells. As shown in Figure 2B, PF-543

doses as low as 1.25 μ M significantly enhanced the effects of both 2 and 4 μ M MTX, relative to either concentration of MTX alone. At 2 μ M MTX, the average percent difference between MTX alone and MTX + PF-543 was 21.05 for 1.25 μ M PF-543 (95%CI: 3.790 to 38.31, $P=0.0054$), 17.5 for 2.5 μ M PF-543 (95% CI: 0.2400 to 34.76, $P=0.0438$) and 24.55 for 5 μ M PF-543 (95% CI: 7.290 to 41.81, $P=0.0006$). At 4 μ M MTX, the average percent difference between MTX alone and MTX + PF-543 was 23.5 for 1.25 μ M PF-543 (95%CI: 6.240 to 40.76, $P=0.0012$), 27.15 for 2.5 μ M PF-543 (95% CI: 9.890 to 44.41, $P<0.0001$) and 28.2 for 5 μ M PF-543 (95% CI: 10.94 to 45.46, $P<0.0001$). ABC significantly enhanced the effects of 4 μ M MTX only at doses of 1.25 and 2.5 μ M. At 4 μ M MTX, the average percent difference between MTX alone and MTX + ABC was 19.1 for 1.25 μ M ABC (95%CI: 1.840 to 36.36, $P=0.0175$), and 23.4 for 2.5 μ M ABC (95% CI: 6.140 to 40.66, $P=0.0012$). The combination of lower doses of PF-543 and ABC showed no additive effects on cell viability, however, the combination of 2.5 μ M PF-543 and 2.5 μ M ABC significantly enhanced the effects of 4 μ M MTX while the combination of 5 μ M PF-543 and 5 μ M ABC significantly enhanced the effects of both 2 and 4 μ M MTX. At 4 μ M MTX, the average percent difference between MTX alone and MTX + 2.5 μ M PF-543 + 2.5 μ M ABC was 23.4 (95% CI: 6.140 to 40.66, $P=0.0012$) and at MTX + 5 μ M PF-543 + 5 μ M ABC was 26.8 (95% CI: 9.540 to 44.06, $P<0.0001$). At 2 μ M MTX, the average percent difference between MTX alone and MTX + 5 μ M PF-543 + 5 μ M ABC was 17.7 (95%CI: 0.4400 to 34.96, $P=0.0392$). Taken together, these data suggest that inhibition of either SphK1 or SphK2 is sufficient to enhance the effects of MTX. These results are consistent with previous studies that demonstrated that targeting either SphK1 or SphK2 using siRNA or shRNA sensitized cancer cells to another anthracycline, doxorubicin (Sankala et al., 2007; Wang et al., 2018).

The SRB assay, as employed, cannot distinguish between the induction of cell death, or induction of growth arrest. Thus, we next examined the temporal expression of cell death markers in response to the combination of MTX+PF-543 in DLD-1 cells, by western blot analysis. As shown in Figure 2C, neither MTX (4 μ M) nor PF-543 (5 μ M) alone induced

PARP/caspase 3 cleavage to a detectable level at 48h, implying that MTX alone, in the range of 1 to 4 μ M, induced cell growth arrest in the SRB assays. Conversely, the combination of MTX+PF-543, at the same concentrations, induced cleavage of PARP and activation/cleavage of caspase 3 beginning at 16h. Together, these results indicate that targeting the SphKs enhances cell death induced by MTX, as has been observed previously for other anthracyclines, such as DOX (Taha et al., 2004; Huwiler et al., 2011; Yao et al., 2012; Leili et al., 2018).

Sphingosine Kinase Inhibition enhances MTX-induced cell surface expression of CRT and ATP release.

Having identified concentrations of SKIs (e.g. PF-543 and ABC) that enhanced cell death in response to MTX, we next determined whether the combination of MTX+SKIs enhanced the cell surface exposure of CRT. Both PF-543 and ABC were employed at concentrations that would inhibit both SphK1 and SphK2, as we have previously determined by direct target engagement assays in whole cells (Hengst et al., 2020). As shown in Figure 3A, PF-543 alone had no effect on the cell surface exposure of CRT in DLD-1 cells, compared to vehicle treated cells, as determined by flow-cytometry employing the above described assay. Minimally effective doses of MTX induced minimal exposure of CRT whereas, these same doses in combination with PF-543, in DLD-1 cells, enhanced CRT exposure determined by flow cytometry. Similar results were observed for PF-543 in MC-38 mouse CRC cells (Figure 3B). Relative to MTX (4 μ M) alone, the addition of PF-543 (5 μ M) significantly increased CRT exposure from a mean fluorescence intensity of 47.03 to 87.37 (40.43 MFI, 95%CI: 18.91 to 61.95, P=0.0014).

To better define the relative contribution of SphK1 and SphK2 inhibition to the enhancement of MTX-induced CRT exposure, we again employed lower, more isoform selective doses of PF-543 and ABC. As shown in Figure 3C, even at the lowest dose tested, PF-543 (1.25 μ M) was able to significantly enhance the exposure of CRT induced by 2 μ M MTX.

Indeed, MTX alone at 2 μ M induced a 6.0 fold increase in exposure of CRT relative to vehicle treatment. The addition of 1.25 μ M PF-543 further enhanced the exposure of CRT (to 10.03 fold) with an average mean fold difference of 4.033 (95% CI: 0.2845 to 7.782, $P=0.0211$). Similarly, ABC at 2.5 μ M further enhanced the exposure of CRT (to 10.1 fold) with an average mean fold difference of 4.1 (95% CI: 0.3511 to 7.849, $P=0.017$).

Importantly, all three combinations of PF-543 and ABC were able to significantly increase CRT exposure relative to either agent alone at 2 μ M MTX. We observed an average mean fold increase of 8.2 from 10.03 for MTX (2 μ M) + PF-543 (1.25 μ M) to 18.23 for MTX (2 μ M) + PF-543 (1.25 μ M) + ABC (1.25 μ M) (95% CI: 4.451 to 11.95, $P<0.0001$) and an average mean fold increase of 9.567 from 8.667 for MTX (2 μ M) + ABC (1.25 μ M) to 18.23 for MTX (2 μ M) + PF-543 (1.25 μ M) + ABC (1.25 μ M) (95% CI: 5.818 to 13.31, $P<0.0001$). Similar results were obtained for the 2.5 μ M combination relative to 2.5 μ M PF-543 alone ($P<0.0001$) and for 2.5 μ M ABC alone ($P<0.0001$).

At 4 μ M MTX, only the combination of 1.25 μ M PF-543 and 1.25 μ M ABC was significantly different than the 4 μ M MTX + PF-543 alone treatments with an average mean fold change of 10.17 from 14.47 for MTX (4 μ M) + PF-543 (1.25 μ M) to 24.63 for MTX (4 μ M) + PF-543 (1.25 μ M) + ABC (1.25 μ M) (95% CI: 6.418 to 13.92, $P<0.0001$). Whereas, all three combinations of 4 μ M MTX + PF-543 + ABC were significant relative to 4 μ M MTX + ABC alone ($P<0.0001$). Together, these data indicate that unlike the effects on cell viability, there is a contribution of both SphK1 and SphK2 inhibition to the enhancement of cell surface CRT exposure.

To extend these observations to the production of other DAMPs, we examined effects of MTX \pm SKIs on the release of ATP into the cell culture medium. As shown in Figure 3D, we also observed an enhancement of ATP release by the combination of MTX with the SKIs (PF-543 and ABC) as compared to single agent treatments in CT-26 cells (average increase of 160 RLU

for ABC+MTX; average RLU 377 vs ABC; average RLU 218; 95% CI: 127.0 to 191.8, $P<0.0001$, average increase of 157 RLU for PF-543+MTX; average RLU 370 vs PF-543; average RLU 213; 95% CI: 124.9 to 189.7, $P<0.0001$) and an average increase of 87 and 94 RLU for either combination (ABC; 377 and PF-543; 370 vs MTX alone; average RLU 283; 95% CI: 62.3 to 127 and 154.7 to 119.6 for ABC and PF-543 respectively, both $P<0.0001$). Together, these results indicate that inhibition of SphK activity enhances MTX-induced production of DAMPs associated with ICD.

SphK inhibition enhances MTX-induced Cer accumulation.

We believe that SphK inhibition enhances MTX-induced cell death by blocking the formation of S1P, leading to the accumulation of its substrate Sph and the subsequent production of Cer from the accumulated pool of Sph (Figure 4A). Thus, we first examined the effects of PF-543 and MTX on production of S1P in DLD-1 cells by LC/MS/MS based sphingolipid metabolite analysis. As shown in Figure 4B, PF-543 alone and MTX+PF-543 significantly reduced production of S1P from an average of 0.00075 pmoles/nmole Pi (Vehicle treatment) to an average of 0.00023 pmoles/nmole Pi (PF-543, 95% CI; 0.000118 to 0.000982 pmoles/nmole Pi, $P=0.0222$) or an average of 0.00030 pmoles/nmole Pi (MTX+PF-543, 95% CI; 0.0000182 to 0.000882 pmoles/nmole Pi, $P=0.0437$) indicating inhibition of the SphKs. Similarly, MTX alone, PF-543 alone, and their combination significantly reduced levels of dhS1P from an average of 0.00085 pmoles/nmole Pi (Vehicle treatment) to an average of 0.00025 pmoles/nmole Pi (MTX, 95% CI; 0.000101 to 0.00110 pmoles/nmole Pi, $P=0.0270$) and an average of 0.00015 pmoles/nmole Pi for both PF-543 and MTX+PF-543 (95%CI; 0.000201 to 0.00120 pmoles/nmole Pi, $P=0.0158$ for both conditions). Interestingly, PF-543 alone, reciprocally induced accumulation of the substrates Sph/dhSph, however, in combination with MTX the levels of Sph/dhSph were reduced. This suggests that SphK inhibition alone does not induce Cer accumulation, but in combination with an agent that induces ER stress, such as

MTX, Sph/dhSph is converted to ceramides. This is consistent with the reported inability of PF-543 to induce apoptosis (Schnute et al., 2012) and with our observation that PF-543 enhances cell death induced by MTX (Figure 2C).

We next examined whether MTX alone or MTX+PF-543 induced Cer accumulation. At a cytostatic dose (4 μ M), MTX induced a modest accumulation of C16:0 Cer, but did not affect other major sphingolipid species (C18:0 and C24:1). However, in combination with PF-543, MTX induced a redistribution of the accumulated sphingolipids with a reduction of PF-543 induced Sph/dhSph, the substrate of the CerS, and a concomitant increase in major Cer species. As shown in Figure 4C, the combination of MTX+PF-543 induced accumulation of C16:0 Cer from an average of 0.754 pmoles/nmole Pi for MTX alone to an average of 2.144 pmoles/nmole Pi for the combination (95%CI; 0.798 to 1.983 pmoles/nmole Pi, P=0.0023). Similarly, C18:0 Cer was increased from 0.073 pmoles/nmole Pi for MTX alone to 0.329 pmoles/nmole Pi for the combination (95% CI; 0.183 to 0.330 pmoles/nmole Pi, P=0.0005) and C24:1 Cer was increased from 0.850 pmoles/nmole Pi for MTX alone to 1.795 pmoles/nmole Pi for the combination (95% CI; 0.437 to 1.453 pmoles/nmole Pi, P=0.0056). Taken together, these data indicate that under conditions favoring the induction of ER stress, such as MTX treatment, inhibition of the SphKs, using PF-543, induces significant increases in levels of Cer.

MTX induces formation of a disulfide bridged dimeric form of CRT.

Studies aimed at characterizing functional domains of human CRT have demonstrated that the N domain contains three cysteine residues, of which Cys146 is present in the reduced form (Hojrup et al., 2001). Further in vitro studies have shown that purified human CRT responds to physical stress such as acidic conditions and high temperatures or denaturing organic agents by forming homodimers through inter-subunit disulfide bond formation of Cys146 in-vitro (Jorgensen et al., 2003). To our knowledge, the oligomeric structure of CRT in response

to ICD-inducing agents has not been examined. To determine if the ER stressor, MTX, could induce oligomerization of CRT, we treated DLD-1 cells and analyzed the oligomeric state of CRT under reducing and non-reducing conditions by western blot analysis.

As shown in Figure 5A, MTX induced a dose dependent formation of a higher molecular weight form of CRT which was consistent with a dimeric complex. Importantly, PF-543 alone had no effect on the oligomeric state of CRT, however, PF-543 (5 μ M) enhanced formation of the apparent CRT dimer at a minimally effective MTX dose (1 μ M). The appearance of the higher molecular weight form of CRT suggested the possibility that MTX \pm PF-543 induced the formation of a disulfide-linked dimeric form of CRT. Thus, we next compared the oligomeric structure of CRT under reducing and non-reducing conditions. Addition of the reducing agent β -mercaptoethanol (β -ME) resulted in collapse of the dimeric form into a monomeric form of CRT (Figure 5B). In contrast to MTX treatment, dimerization did not occur in untreated cells consistent with previous results. These results show that MTX induces disulfide-bridged dimerization of CRT in cells.

MTX-Induced Dimerized CRT localizes to detergent insoluble plasma membranes.

Fluorescence microscopy studies have shown that CRT displayed by apoptotic cells localizes to cholesterol rich region in the GM-1 ganglioside lipid rafts microdomain (Gardai et al., 2005). Further studies demonstrated that MTX-induced CRT translocates to lipid rafts region and is decreased by depletion of cholesterol (Garg et al., 2012b). To determine the oligomeric structure of CRT localized in lipid rafts, in response to MTX treatment, we isolated the total membrane lipid raft fraction by taking advantage of its insolubility in the non-ionic detergent Triton X-100 at 4°C (Magee and Parmryd, 2003). Given that PF-543 enhances MTX-induced dimerization of CRT, we restricted our focus to determining the effects of the combined

MTX+PF-543 treatment on the lipid raft localization of CRT. MTX+PF-543 treated DLD-1 cells were fractionated by differential centrifugation as shown in Figure 6A. Cytosolic, Triton X-100 soluble and Triton X-100 detergent insoluble membrane fractions were subjected to western blot analysis under non-reducing conditions.

Consistent with the observations in whole cell lysates above, CRT in untreated cells remained monomeric, whereas, MTX+PF-543 treatment induced dimerization of CRT in all 3 subcellular fractions (Figure 6B). Importantly, only dimerized CRT was present in the Triton X-100 detergent insoluble membrane fraction. The monomeric form on the other hand was undetectable in this region. These results corroborate the reported findings of microscopic studies that CRT displayed by dying or dead cells localizes to lipid raft microdomains (Gardai et al., 2005; Gardai et al., 2006). They further suggest that lipid raft localized, MTX-induced CRT is a disulfide-linked dimer.

The plasma membrane lipid raft is highly enriched in sphingolipids and our data indicates that SphK inhibition enhances MTX-induced Cer accumulation suggesting that cell surface exposed CRT preferentially associates with Cer-enriched membrane microdomains. Thus, inhibition of Cer formation should affect cell surface exposure of CRT. We, therefore, inhibited Cer formation using the Cer synthase inhibitor, Fumonisin B1, and examined the association of dimerized CRT with the Triton X-100 detergent insoluble membrane fraction of DLD-1 cells treated with MTX±PF-543. Consistent with the results obtained above, MTX alone modestly relocalized a dimerized form of CRT to the Triton X-100 insoluble membrane fraction which was enhanced by SphK inhibition/Cer accumulation in combination with PF-543 (Figure 6C). Importantly, Fumonisin B1 abrogated the effects of SphK inhibition on CRT relocalization to the Triton X-100 insoluble membrane fraction indicating that enhanced Cer formation, and not

inhibition of S1P production is responsible for the observed generation of dimerized, plasma membrane localized CRT.

DISCUSSION

Herein, we report, for the first time, that inhibition of the SphKs enhances the cytotoxicity, cell surface expression of CRT and secretion of ATP induced by low doses of the anthracycline, MTX, in human and mouse CRC cell lines. This enhanced production of DAMPs, by SphK inhibition, implies that the sphingolipid metabolic pathway and Cer accumulation, in particular, is an important, previously unrecognized factor that is critical to the processes of ICD. As mentioned above, numerous examples in the literature suggest an intersection between the cellular effects of Cer accumulation and the mechanism of cell death associated with ICD. Our current results suggest that Cer accumulation, through SphK inhibition, might enhance the immunogenicity of known ICD-inducing agents including clinically relevant chemotherapeutic agents, such as MTX, ionizing radiation and photo-dynamic therapy. Whether Cer accumulation is a common feature of all ICD-inducing agents or is unique to certain subsets of agents/therapies is unknown at this time.

The mechanism(s) associated with Cer induced cell death have been thoroughly dissected, for decades. Cer accumulation has canonically been thought to induce apoptosis, a form of non-immunogenic or tolerogenic cell death that does not engage the innate/adaptive immune response (Obeid et al., 1993). Our results imply that ICD may be a “non-canonical” form of Cer-associated cell death. Previous studies have demonstrated that exogenously delivered non-natural Cer analogs (C₂-Cer) were not able to induce the cell surface exposure of CRT on their own (Obeid et al., 2007b). A significant portion of exogenously delivered Cer analogs are anabolically converted to higher order sphingolipids (e.g. C₂-Sphingomyelin and C₂-Glucosylceramide) (Chapman et al., 2010). Another significant portion of the C₂-Cer can be

deacylated to remove the C₂ acyl chain and form Sph through the actions of the ceramidases (Gault et al., 2010). The resultant Sph can be rapidly converted to S1P by the SphKs. This pool of Sph can also be reacylated to form natural Cer species at the ER. Given the many possible fates, it is possible to imagine a scenario where exogenously added Cer analogs could be cytotoxic to cancer cells and yet the levels of natural Cer species do not reach a critical threshold to influence the local environment in the ER (i.e. ER stress) and induce cell surface expression of CRT.

In this study, we demonstrate that moderately effective doses of MTX modestly induce the production of C16:0 Cer and enhance the production of all Cer species when the conversion of Sph to S1P is blocked by inhibition of the SphKs. This is consistent with the idea that when S1P formation is blocked, Sph is rerouted to the generation of natural Cer species in the ER, the amplification of ER stress and the subsequent cell surface exposure of CRT. It is also possible that S1P may have a protective “anti-ICD” effect, however, SphK inhibition alone induces Sph accumulation rather than Cer accumulation suggesting that ER stress, induced by MTX for example, is a prerequisite for Cer production. Further study will be required to firmly establish the role of Cer in ICD.

CRT normally resides in the lumen of the endoplasmic reticulum where its functions include calcium regulation and assisting protein folding (Michalak et al., 1999; Michalak et al., 2009; Lu et al., 2015). In response to agents, such as photodynamic therapy and the anthracyclines (e.g. MTX and doxorubicin), that induce ICD, CRT relocates to the extracellular surface of tumor cells eliciting an anti-cancer immunological response by cells of the innate/adaptive immune system (Obeid, 2008; Panaretakis et al., 2009; Garg et al., 2012b). For example, *in vitro* studies have shown that cancer cells undergoing cell death after exposure to MTX stimulate maturation and activation of dendritic cells (DC) (Garg et al., 2012b).

Furthermore, when these cells are injected into immunocompetent mice (i.e. vaccination assays) they result in a protective anti-cancer immune response, to a subsequent live cell challenge (Obeid et al., 2007b; Zitvogel et al., 2010). Analyses of the plasma membrane proteome revealed that the immunogenically dying cells expose CRT on their cell surface while apoptotic (non-immunogenic) cells did not, indicating that the immunogenicity of MTX relies at least in part on its ability to induce cell surface exposed CRT (Obeid et al., 2007b). This idea has been supported by studies in which depletion of CRT by siRNA or use of neutralizing antibodies averted DC stimulation and abrogated antitumor immunity.

Our results demonstrate that induction of ER stress by MTX results in formation of disulfide-bridged dimers of CRT which localize to detergent insoluble, sphingolipid rich, lipid raft membrane fraction of the plasma membrane. The formation of this dimeric form of CRT was also enhanced by inhibition of the sphingolipid metabolic pathway. Previous investigations have reported that human CRT possesses three cysteine residues, two of which are involved in intra-subunit covalent bonds while the third, Cys146, is present in the reduced form. In vitro studies have demonstrated that subjecting CRT to denaturing conditions, such as low pH and high heat or calcium depleting agents, resulted in unmasking Cys146 and CRT homodimer formation (Jorgensen et al., 2003; Rizvi et al., 2004). MTX is known to increase production of reactive oxygen species (ROS) in the ER (Garg et al., 2012a; Garg et al., 2012b). ROS may promote the unfolding of CRT and solvent exposure of the free SH of Cys146 where it could disulfide link with another CRT thiol group. Other studies have demonstrated that ICD-induced cell surface expressed CRT associates with another, normally ER resident chaperone ERp57 (Obeid, 2008; Panaretakis et al., 2009).

At this juncture, we cannot preclude the possibility that the “dimeric” form of CRT represents a hetero-dimeric association between CRT (55kDa) and ERp57 (57kDa).

Alternatively, a homo-dimer of CRT could interact with monomeric ERp57 as it translocates to the cell surface. The possibility also exists that homo-dimers of CRT could form higher order oligomeric structures through non-covalent dimer:dimer interactions. Such oligomeric interactions could serve to increase the local concentration of cell surface exposed CRT. Coupled with the selective localization of cell surface exposed CRT within the lipid raft regions of plasma membrane, dimerization/oligomerization would serve to enhance the likelihood of recognition/engulfment by DCs. Further study will be required to fully elucidate the oligomeric structure and binding partners of CRT at the cell surface and how these interactions affect immunogenicity of cells undergoing ICD.

Taken together, our findings suggest that immunogenic CRT is a disulfide bridged dimer and indicate a role for Cer accumulation in the mechanism by which ICD inducers render cancer cells immunogenic. Detailed molecular studies should help to clarify the role of Cer in ICD as well as distinguish where it diverges from its classical role in apoptosis. Future studies will also be directed to provide in-vivo demonstration of the role of SphK inhibition/Cer accumulation in induction of ICD by the “gold-standard” vaccination assay method in immunocompetent mouse syngeneic models of CRC (Humeau et al., 2019).

Anthracyclines, such as MTX, doxorubicin, daunorubicin, etc., are routinely employed in combinatorial chemotherapeutic regimens for a number of cancers. They induce CRT exposure as an “off-target” effect separate from their topoisomerase inhibitory activity. Given that they are typically employed at concentrations approaching the maximum tolerated dosage, it is possible that they induce immunosuppression by depletion of the very immune cells needed to mount an immunogenic attack on the cancer cells (Vanmeerbeek et al., 2020). Thus, current strategies employing the anthracyclines have the potential for overt toxicity and may be self-limiting in their ability to activate the innate/adaptive immune response. The addition of a SphK inhibitor, such

as PF-543 or ABC294640 (currently under Phase I/II clinical trials) could allow for the use of less overtly toxic doses and amplify the effects of ICD-inducing agents, such as MTX, in standard-of care therapies or in new chemotherapeutic regimens specifically tailored to maximize the induction of ICD/activation of the innate adaptive immune response.

CONFLICT OF INTEREST

No author has an actual or perceived conflict of interest with the contents of this article.

AUTHOR CONTRIBUTIONS

Participated in research design: Nduwumwami, Hengst and Yun.

Conducted experiments: Nduwumwami, Hengst and Yun.

Performed statistical data analysis: Nduwumwami.

Wrote or contributed to the writing of the manuscript: Nduwumwami, Hengst and Yun.

REFERENCES

- Beverly LJ, Howell LA, Hernandez-Corbacho M, Casson L, Chipuk JE and Siskind LJ (2013) BAK activation is necessary and sufficient to drive ceramide synthase-dependent ceramide accumulation following inhibition of BCL2-like proteins. *The Biochemical journal* **452**:111-119.
- Bezu L, Sauvat A, Humeau J, Gomes-da-Silva LC, Iribarren K, Forveille S, Garcia P, Zhao L, Liu P, Zitvogel L, Senovilla L, Kepp O and Kroemer G (2018) eIF2alpha phosphorylation is pathognomonic for immunogenic cell death. *Cell death and differentiation* **25**:1375-1393.
- Chapman JV, Gouaze-Andersson V, Messner MC, Flowers M, Karimi R, Kester M, Barth BM, Liu X, Liu YY, Giuliano AE and Cabot MC (2010) Metabolism of short-chain ceramide by human cancer cells--implications for therapeutic approaches. *Biochemical pharmacology* **80**:308-315.
- Cuvillier O, Nava VE, Murthy SK, Edsall LC, Levade T, Milstien S and Spiegel S (2001) Sphingosine generation, cytochrome c release, and activation of caspase-7 in doxorubicin-induced apoptosis of MCF7 breast adenocarcinoma cells. *Cell death and differentiation* **8**:162-171.
- Cuvillier O, Pirianov G, Kleuser B, Vanek PG, Coso OA, Gutkind S and Spiegel S (1996) Suppression of ceramide-mediated programmed cell death by sphingosine-1-phosphate. *Nature* **381**:800-803.
- French KJ, Zhuang Y, Maines LW, Gao P, Wang W, Beljanski V, Upson JJ, Green CL, Keller SN and Smith CD (2010) Pharmacology and antitumor activity of ABC294640, a selective inhibitor of sphingosine kinase-2. *J Pharmacol Exp Ther* **333**:129-139.
- Galluzzi L, Buque A, Kepp O, Zitvogel L and Kroemer G (2015) Immunological Effects of Conventional Chemotherapy and Targeted Anticancer Agents. *Cancer cell* **28**:690-714.
- Galluzzi L, Buque A, Kepp O, Zitvogel L and Kroemer G (2017) Immunogenic cell death in cancer and infectious disease. *Nat Rev Immunol* **17**:97-111.
- Galluzzi L, Chan TA, Kroemer G, Wolchok JD and Lopez-Soto A (2018) The hallmarks of successful anticancer immunotherapy. *Science translational medicine* **10**.
- Gardai SJ, Bratton DL, Ogden CA and Henson PM (2006) Recognition ligands on apoptotic cells: a perspective. *J Leukoc Biol* **79**:896-903.
- Gardai SJ, McPhillips KA, Frasch SC, Janssen WJ, Starefeldt A, Murphy-Ullrich JE, Bratton DL, Oldenborg PA, Michalak M and Henson PM (2005) Cell-surface calreticulin initiates clearance of viable or apoptotic cells through trans-activation of LRP on the phagocyte. *Cell* **123**:321-334.
- Garg AD, Krysko DV, Vandenabeele P and Agostinis P (2012a) The emergence of phox-ER stress induced immunogenic apoptosis. *Oncoimmunology* **1**:786-788.
- Garg AD, Krysko DV, Verfaillie T, Kaczmarek A, Ferreira GB, Marysael T, Rubio N, Firczuk M, Mathieu C, Roebroek AJ, Annaert W, Golab J, de Witte P, Vandenabeele P and Agostinis P (2012b) A novel pathway combining calreticulin exposure and ATP secretion in immunogenic cancer cell death. *The EMBO journal* **31**:1062-1079.
- Gault CR, Obeid LM and Hannun YA (2010) An overview of sphingolipid metabolism: from synthesis to breakdown. *Advances in experimental medicine and biology* **688**:1-23.
- Gong L, Yang B, Xu M, Cheng B, Tang X, Zheng P, Jing Y and Wu GJ (2014) Bortezomib-induced apoptosis in cultured pancreatic cancer cells is associated with ceramide production. *Cancer chemotherapy and pharmacology* **73**:69-77.
- Grammatikos G, Teichgraber V, Carpinteiro A, Trarbach T, Weller M, Hengge UR and Gulbins E (2007) Overexpression of acid sphingomyelinase sensitizes glioma cells to chemotherapy. *Antioxidants & redox signaling* **9**:1449-1456.

- Gucluler G, Piskin O and Baran Y (2011) The roles of antiapoptotic sphingosine kinase-1 and glucosylceramide genes in drug induced cell death of MCF-7 breast cancer cells. *Journal of BUON : official journal of the Balkan Union of Oncology* **16**:646-651.
- Hazar-Rethinam M, de Long LM, Gannon OM, Topkas E, Boros S, Vargas AC, Dzienis M, Mukhopadhyay P, Simpson F, Endo-Munoz L and Saunders NA (2015) A novel E2F/sphingosine kinase 1 axis regulates anthracycline response in squamous cell carcinoma. *Clinical cancer research : an official journal of the American Association for Cancer Research* **21**:417-427.
- Hengst JA, Dick TE, Smith CD and Yun JK (2020) Analysis of selective target engagement by small-molecule sphingosine kinase inhibitors using the Cellular Thermal Shift Assay (CETSA). *Cancer biology & therapy* **21**:841-852.
- Hengst JA, Guilford JM, Fox TE, Wang X, Conroy EJ and Yun JK (2009) Sphingosine kinase 1 localized to the plasma membrane lipid raft microdomain overcomes serum deprivation induced growth inhibition. *Archives of biochemistry and biophysics* **492**:62-73.
- Hojrup P, Roepstorff P and Houen G (2001) Human placental calreticulin characterization of domain structure and post-translational modifications. *Eur J Biochem* **268**:2558-2565.
- Humeau J, Lévesque S, Kroemer G and Pol JG (2019) Gold Standard Assessment of Immunogenic Cell Death in Oncological Mouse Models, in *Cancer Immunossurveillance: Methods and Protocols* (López-Soto A and Folgueras AR eds) pp 297-315, Springer New York, New York, NY.
- Huwiler A, Kotelevets N, Xin C, Pastukhov O, Pfeilschifter J and Zangemeister-Wittke U (2011) Loss of sphingosine kinase-1 in carcinoma cells increases formation of reactive oxygen species and sensitivity to doxorubicin-induced DNA damage. *Br J Pharmacol* **162**:532-543.
- Jorgensen CS, Ryder LR, Steino A, Hojrup P, Hansen J, Beyer NH, Heegaard NH and Houen G (2003) Dimerization and oligomerization of the chaperone calreticulin. *Eur J Biochem* **270**:4140-4148.
- Kepp O, Senovilla L, Zitvogel L, Kroemer G and Galluzzi L (2014) Consensus guidelines for the detection of immunogenic cell death. *Oncoimmunology* **3**:e955691.
- Kim HJ, Oh JE, Kim SW, Chun YJ and Kim MY (2008) Ceramide induces p38 MAPK-dependent apoptosis and Bax translocation via inhibition of Akt in HL-60 cells. *Cancer letters* **260**:88-95.
- Korbelik M, Banath J, Sun J, Canals D, Hannun YA and Separovic D (2014) Ceramide and sphingosine-1-phosphate act as photodynamic therapy-elicited damage-associated molecular patterns: cell surface exposure. *International immunopharmacology* **20**:359-365.
- Leili H, Nasser S, Nadereh R, Siavoush D and Pouran K (2018) Sphingosine kinase-2 Inhibitor ABC294640 Enhances Doxorubicin-Induced Apoptosis of NSCLC Cells via Altering Survivin Expression. *Drug Res (Stuttg)* **68**:45-53.
- Lu YC, Weng WC and Lee H (2015) Functional roles of calreticulin in cancer biology. *Biomed Res Int* **2015**:526524.
- Lucci A, Han TY, Liu YY, Giuliano AE and Cabot MC (1999a) Modification of ceramide metabolism increases cancer cell sensitivity to cytotoxics. *International journal of oncology* **15**:541-546.
- Lucci A, Han TY, Liu YY, Giuliano AE and Cabot MC (1999b) Multidrug resistance modulators and doxorubicin synergize to elevate ceramide levels and elicit apoptosis in drug-resistant cancer cells. *Cancer* **86**:300-311.
- Magee AI and Parmryd I (2003) Detergent-resistant membranes and the protein composition of lipid rafts. *Genome Biol* **4**:234.
- Marshall HT and Djamgoz MBA (2018) Immuno-Oncology: Emerging Targets and Combination Therapies. *Frontiers in oncology* **8**:315.

- Michalak M, Corbett EF, Mesaali N, Nakamura K and Opas M (1999) Calreticulin: one protein, one gene, many functions. *The Biochemical journal* **344 Pt 2**:281-292.
- Michalak M, Groenendyk J, Szabo E, Gold LI and Opas M (2009) Calreticulin, a multi-process calcium-buffering chaperone of the endoplasmic reticulum. *The Biochemical journal* **417**:651-666.
- Nemoto S, Nakamura M, Osawa Y, Kono S, Itoh Y, Okano Y, Murate T, Hara A, Ueda H, Nozawa Y and Banno Y (2009) Sphingosine kinase isoforms regulate oxaliplatin sensitivity of human colon cancer cells through ceramide accumulation and Akt activation. *The Journal of biological chemistry* **284**:10422-10432.
- Nica AF, Tsao CC, Watt JC, Jiffar T, Kurinna S, Jurasz P, Konopleva M, Andreeff M, Radomski MW and Ruvalo PP (2008) Ceramide promotes apoptosis in chronic myelogenous leukemia-derived K562 cells by a mechanism involving caspase-8 and JNK. *Cell Cycle* **7**:3362-3370.
- Obeid LM, Linardic CM, Karolak LA and Hannun YA (1993) Programmed cell death induced by ceramide. *Science* **259**:1769-1771.
- Obeid M (2008) ERP57 membrane translocation dictates the immunogenicity of tumor cell death by controlling the membrane translocation of calreticulin. *J Immunol* **181**:2533-2543.
- Obeid M, Panaretakis T, Joza N, Tufi R, Tesniere A, van Endert P, Zitvogel L and Kroemer G (2007a) Calreticulin exposure is required for the immunogenicity of gamma-irradiation and UVC light-induced apoptosis. *Cell death and differentiation* **14**:1848-1850.
- Obeid M, Tesniere A, Ghiringhelli F, Fimia GM, Apetoh L, Perfettini JL, Castedo M, Mignot G, Panaretakis T, Casares N, Metivier D, Larochette N, van Endert P, Ciccocanti F, Piacentini M, Zitvogel L and Kroemer G (2007b) Calreticulin exposure dictates the immunogenicity of cancer cell death. *Nature medicine* **13**:54-61.
- Ohta H, Sweeney EA, Masamune A, Yatomi Y, Hakomori S and Igarashi Y (1995) Induction of apoptosis by sphingosine in human leukemic HL-60 cells: a possible endogenous modulator of apoptotic DNA fragmentation occurring during phorbol ester-induced differentiation. *Cancer research* **55**:691-697.
- Panaretakis T, Kepp O, Brockmeier U, Tesniere A, Bjorklund AC, Chapman DC, Durchschlag M, Joza N, Pierron G, van Endert P, Yuan J, Zitvogel L, Madeo F, Williams DB and Kroemer G (2009) Mechanisms of pre-apoptotic calreticulin exposure in immunogenic cell death. *The EMBO journal* **28**:578-590.
- Park MA, Walker T, Martin AP, Allegood J, Vozhilla N, Emdad L, Sarkar D, Rahmani M, Graf M, Yacoub A, Koumenis C, Spiegel S, Curiel DT, Voelkel-Johnson C, Grant S, Fisher PB and Dent P (2009) MDA-7/IL-24-induced cell killing in malignant renal carcinoma cells occurs by a ceramide/CD95/PERK-dependent mechanism. *Molecular cancer therapeutics* **8**:1280-1291.
- Park MA, Zhang G, Martin AP, Hamed H, Mitchell C, Hylemon PB, Graf M, Rahmani M, Ryan K, Liu X, Spiegel S, Norris J, Fisher PB, Grant S and Dent P (2008a) Vorinostat and sorafenib increase ER stress, autophagy and apoptosis via ceramide-dependent CD95 and PERK activation. *Cancer biology & therapy* **7**:1648-1662.
- Park MA, Zhang G, Norris J, Hylemon PB, Fisher PB, Grant S and Dent P (2008b) Regulation of autophagy by ceramide-CD95-PERK signaling. *Autophagy* **4**:929-931.
- Paugh SW, Paugh BS, Rahmani M, Kapitonov D, Almenara JA, Kordula T, Milstien S, Adams JK, Zipkin RE, Grant S and Spiegel S (2008) A selective sphingosine kinase 1 inhibitor integrates multiple molecular therapeutic targets in human leukemia. *Blood* **112**:1382-1391.
- Qiu L, Zhou C, Sun Y, Di W, Scheffler E, Healey S, Wanebo H, Kouttab N, Chu W and Wan Y (2006) Paclitaxel and ceramide synergistically induce cell death with transient activation of EGFR and ERK pathway in pancreatic cancer cells. *Oncology reports* **16**:907-913.

- Rath G, Schneider C, Langlois B, Sartelet H, Morjani H, Btaouri HE, Dedieu S and Martiny L (2009) De novo ceramide synthesis is responsible for the anti-tumor properties of camptothecin and doxorubicin in follicular thyroid carcinoma. *The international journal of biochemistry & cell biology* **41**:1165-1172.
- Ren X and Su C (2020) Sphingosine kinase 1 contributes to doxorubicin resistance and glycolysis in osteosarcoma. *Mol Med Rep* **22**:2183-2190.
- Rizvi SM, Mancino L, Thammavongsa V, Cantley RL and Raghavan M (2004) A polypeptide binding conformation of calreticulin is induced by heat shock, calcium depletion, or by deletion of the C-terminal acidic region. *Molecular cell* **15**:913-923.
- Sakakura C, Sweeney E, Shirahama T, Ruan F, Solca F, Kohno M, Hakomori S, Fischer E and Igarashi Y (1997) Inhibition of MAP kinase by sphingosine and its methylated derivative, N,N-dimethylsphingosine. *International journal of oncology* **11**:31-39.
- Sankala HM, Hait NC, Paugh SW, Shida D, Lepine S, Elmore LW, Dent P, Milstien S and Spiegel S (2007) Involvement of sphingosine kinase 2 in p53-independent induction of p21 by the chemotherapeutic drug doxorubicin. *Cancer research* **67**:10466-10474.
- Schnute ME, McReynolds MD, Kasten T, Yates M, Jerome G, Rains JW, Hall T, Chrencik J, Kraus M, Cronin CN, Saabye M, Highkin MK, Broadus R, Ogawa S, Cukyne K, Zawadzke LE, Peterkin V, Iyanar K, Scholten JA, Wendling J, Fujiwara H, Nemirovskiy O, Wittwer AJ and Nagiec MM (2012) Modulation of cellular S1P levels with a novel, potent and specific inhibitor of sphingosine kinase-1. *The Biochemical journal* **444**:79-88.
- Shirahama T, Sakakura C, Sweeney EA, Ozawa M, Takemoto M, Nishiyama K, Ohi Y and Igarashi Y (1997) Sphingosine induces apoptosis in androgen-independent human prostatic carcinoma DU-145 cells by suppression of bcl-X(L) gene expression. *FEBS letters* **407**:97-100.
- Siskind LJ, Mullen TD, Romero Rosales K, Clarke CJ, Hernandez-Corbacho MJ, Edinger AL and Obeid LM (2010) The BCL-2 protein BAK is required for long-chain ceramide generation during apoptosis. *The Journal of biological chemistry* **285**:11818-11826.
- Sweeney EA, Sakakura C, Shirahama T, Masamune A, Ohta H, Hakomori S and Igarashi Y (1996) Sphingosine and its methylated derivative N,N-dimethylsphingosine (DMS) induce apoptosis in a variety of human cancer cell lines. *International journal of cancer* **66**:358-366.
- Taha TA, Osta W, Kozhaya L, Bielawski J, Johnson KR, Gillanders WE, Dbaibo GS, Hannun YA and Obeid LM (2004) Down-regulation of sphingosine kinase-1 by DNA damage: dependence on proteases and p53. *The Journal of biological chemistry* **279**:20546-20554.
- Truman JP, Garcia-Barros M, Obeid LM and Hannun YA (2014) Evolving concepts in cancer therapy through targeting sphingolipid metabolism. *Biochimica et biophysica acta* **1841**:1174-1188.
- Vanmeerbeek I, Sprooten J, De Ruyscher D, Tejpar S, Vandenberghe P, Fucikova J, Spisek R, Zitvogel L, Kroemer G, Galluzzi L and Garg AD (2020) Trial watch: chemotherapy-induced immunogenic cell death in immuno-oncology. *Oncoimmunology* **9**:1703449.
- Vichai V and Kirtikara K (2006) Sulforhodamine B colorimetric assay for cytotoxicity screening. *Nature protocols* **1**:1112-1116.
- Walker T, Mitchell C, Park MA, Yacoub A, Graf M, Rahmani M, Houghton PJ, Voelkel-Johnson C, Grant S and Dent P (2009) Sorafenib and vorinostat kill colon cancer cells by CD95-dependent and -independent mechanisms. *Molecular pharmacology* **76**:342-355.
- Wallington-Beddoe CT, Bennett MK, Vandyke K, Davies L, Zebol JR, Moretti PAB, Pitman MR, Hewett DR, Zannettino ACW and Pitson SM (2017) Sphingosine kinase 2 inhibition synergises with bortezomib to target myeloma by enhancing endoplasmic reticulum stress. *Oncotarget* **8**:43602-43616.

- Wang S, Liang Y, Chang W, Hu B and Zhang Y (2018) Triple Negative Breast Cancer Depends on Sphingosine Kinase 1 (SphK1)/Sphingosine-1-Phosphate (S1P)/Sphingosine 1-Phosphate Receptor 3 (S1PR3)/Notch Signaling for Metastasis. *Med Sci Monit* **24**:1912-1923.
- Wang Z, Wen L, Zhu F, Wang Y, Xie Q, Chen Z and Li Y (2017) Overexpression of ceramide synthase 1 increases C18-ceramide and leads to lethal autophagy in human glioma. *Oncotarget* **8**:104022-104036.
- Wernitznig D, Kiakos K, Del Favero G, Harrer N, Machat H, Osswald A, Jakupiec MA, Wernitznig A, Sommergruber W and Keppler BK (2019) First-in-class ruthenium anticancer drug (KP1339/IT-139) induces an immunogenic cell death signature in colorectal spheroids in vitro. *Metallomics* **11**:1044-1048.
- Yao C, Wu S, Li D, Ding H, Wang Z, Yang Y, Yan S and Gu Z (2012) Co-administration phenoxodiol with doxorubicin synergistically inhibit the activity of sphingosine kinase-1 (SphK1), a potential oncogene of osteosarcoma, to suppress osteosarcoma cell growth both in vivo and in vitro. *Mol Oncol* **6**:392-404.
- Zitvogel L, Kepp O, Senovilla L, Menger L, Chaput N and Kroemer G (2010) Immunogenic tumor cell death for optimal anticancer therapy: the calreticulin exposure pathway. *Clinical cancer research : an official journal of the American Association for Cancer Research* **16**:3100-3104.

FOOTNOTES

This work was supported by the Four Diamonds Fund of the Pennsylvania State University (J.K.Y.) and by the Jake Gittlen Memorial Golf Tournament (J.K.Y.).

FIGURE LEGENDS

Figure 1: MTX-induced ER stress mediates cell surface exposure of CRT in DLD-1 cells.

(A). Representative results of DLD-1 cells treated, in triplicate, with MTX (2 μ M) or cisplatin (40 μ M) for 48h. Cell surface exposed CRT was quantified by flow cytometry (MFI: mean fluorescence intensity) (n=3). Statistical analysis was performed using one-way ANOVA followed by Tukey's multiple comparison test. (*) Asterisks indicate significant changes as reported in results section. (B). Representative immunoblot of eIF2 α phosphorylated on serine 51 (p-eIF2 α), total eIF2 α and the loading control GAPDH using appropriate antibodies.

Figure 2. Targeted inhibition of the SphKs enhances MTX induced cell death. (A-B).

Representative results of cell viability SRB assays performed in triplicate (n=2). (A). Mouse CRC CT-26 cells were treated with the indicated SKIs and/or MTX at the indicated concentrations for 48 h. (*) Asterisks are color coded to indicate significant changes as reported in results section. (B) Human DLD-1 CRC cells were treated with the indicated SKIs and/or MTX at the indicated concentrations for 48h. (*) Asterisks indicate significant changes at 2 μ M MTX and (#) hashtags indicate significant changes at 4 μ M MTX as reported in results section. (C). Representative immunoblot analysis of cleaved PARP and cleaved caspase 3. DLD-1 cells were treated with vehicle (V), MTX (M; 4 μ M) and/or PF-543 (P; 5 μ M) for the times indicated. GAPDH was employed as a loading control.

Figure 3. Targeted inhibition of the SphKs enhance the production of ICD-associated DAMPS. (A).

Representative histograms of individual DLD-1, cell samples treated with MTX and/or PF-543 at the indicated concentrations for 48 h. (B). Representative results of MC-38 cells treated with MTX (1 μ M) \pm PF-543 (5 μ M) (n=3). (*) Asterisks indicate significant changes as

reported in results section.(C). Representative results of DLD-1 cells treated with MTX (2 and 4 μ M) \pm SKIs (PF-543 1.25, 2.5 and 5 μ M, ABC294640 1.25, 2.5 and 5 μ M, or their combinations) (n=3). (*) Asterisks indicate significant changes in combination with PF-543 and (#) hashtags indicate significant changes in combination with ABC as reported in results section.(D). Representative results of ATP release determined, in triplicate, by ENLITEN ATP assay in CT-26 cells (n=2). (*) Asterisks indicate significant changes as reported in results section. **A-C**). Cell surface exposed CRT production was determined by flow cytometry using PE conjugated anti-CRT antibodies. **(B-D)**. Statistical analysis was performed using one-way ANOVA followed by Tukey's multiple comparison test.

Figure 4: Sphingosine Kinase Inhibition enhances MTX-induced Cer formation. **(A)**. Schematic representation of the sphingolipid metabolic pathway. CerS; Ceramide Synthases 1-6, CDase; Acid, Alkaline and Neutral Ceramidase, SGPP; S1P phosphatases 1 and 2, S1PL; S1P Lyase. **(B and C)**. Sphingolipidomic analysis was conducted on DLD-1 cell samples treated with MTX (4 μ M) and/or PF-543 (5 μ M) for 24h (n=3). Values are presented as pmoles sphingolipid/nmole inorganic phosphate (pmole/nmole Pi). Statistical analysis was performed using one-way ANOVA followed by Tukey's multiple comparison test. (*) Asterisks indicate significant changes as reported in results section. **(B)**. Levels of dhS1P and S1P. **(C)**. Levels of C16:0, C18:0 and C24:1 Cer, dhSph and Sph.

Figure 5: Induction of dimerization of calreticulin in MTX-dose dependent manner. **(A)**. CRT disulfide linked dimer formation was assessed in DLD-1 whole cell lysates upon MTX-dose dependent treatment, 5 μ M PF-543 alone and in the presence of 1 μ M MTX + 5 μ M PF-543 by immunoblot using anti-CRT antibodies. Vinculin was employed as a loading control (n=3). **(B)**. CRT dimer formation was examined in the presence and absence of MTX (4 μ M) under non-reducing (- β -ME) or reducing (+ β -ME) conditions by immunoblot using anti-CRT antibodies (n=3).

Figure 6: Disulfide linked CRT dimer localizes to lipid raft microdomains. (A). Subcellular fractionation scheme using differential centrifugation. (B). Cytosolic (C), Triton X-100 soluble (TS) and Triton X-100 insoluble (TI) subcellular fractions of DLD-1 cells treated with either vehicle or MTX (4 μ M) + PF-543 (5 μ M) were subjected to non-reducing conditions and analyzed by immunoblot using anti-CRT antibodies (n=3). (C) Subcellular fractionation was performed on DLD-1 cells treated with vehicle, MTX (4 μ M), PF-543 (5 μ M) or their combination in the presence and absence of Fumonisin B1 (70 μ M). The TI fraction was analyzed for the presence of dimerized CRT by western blot analysis. Caveolin 1 represents a loading control and marker for the TI fraction (n=3).

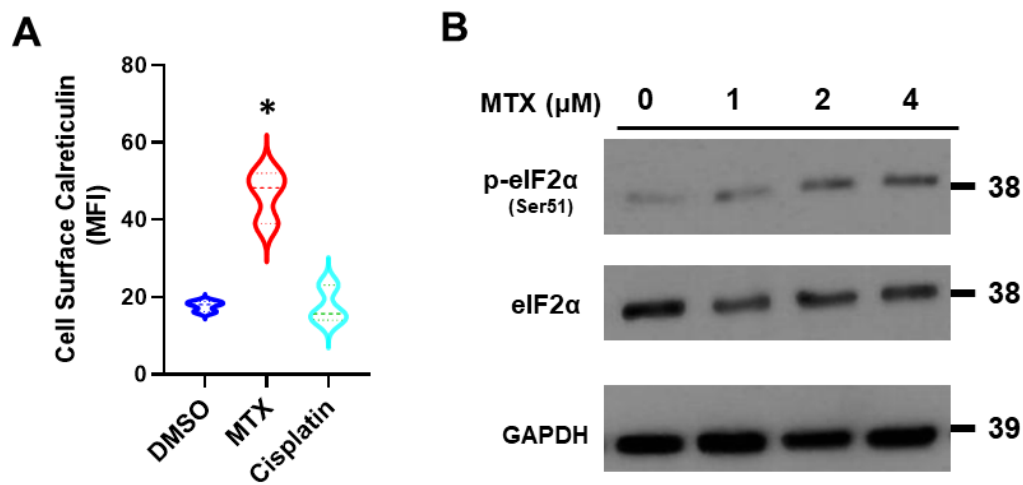
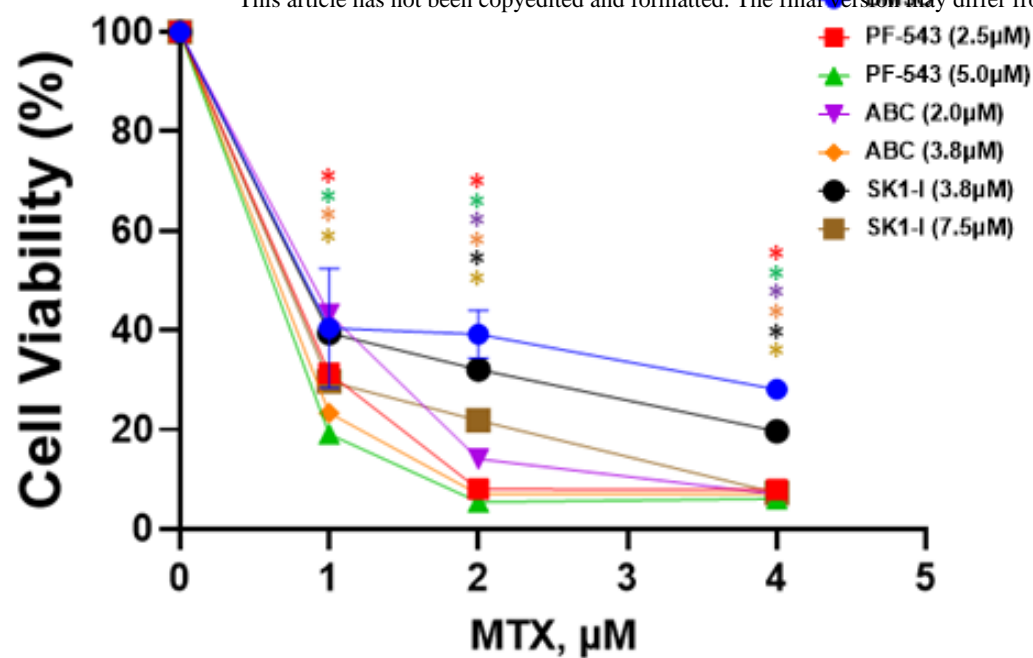
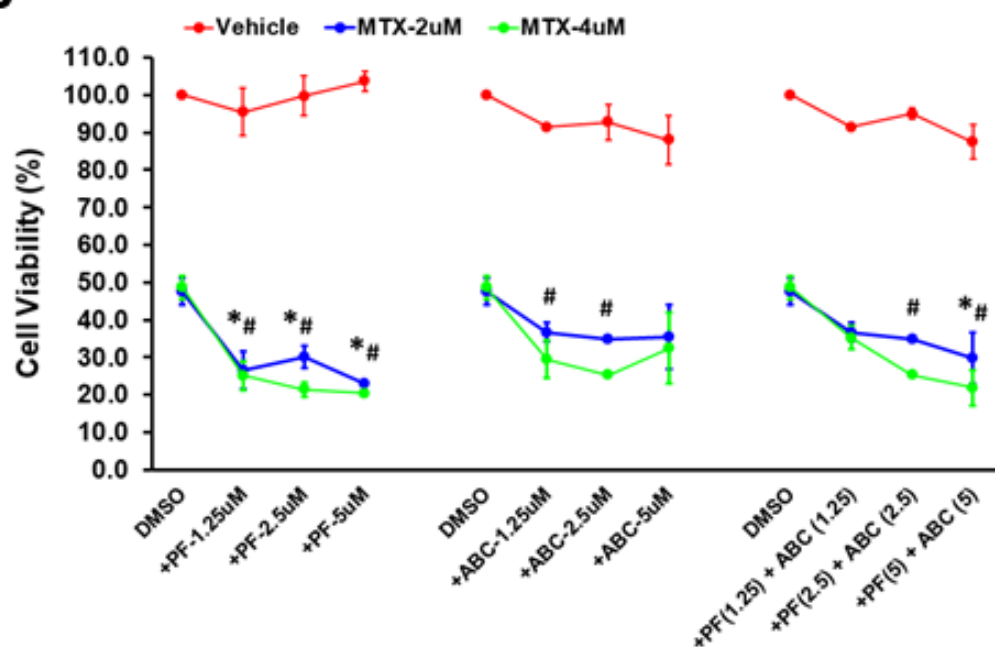


Figure 1

A



B



C

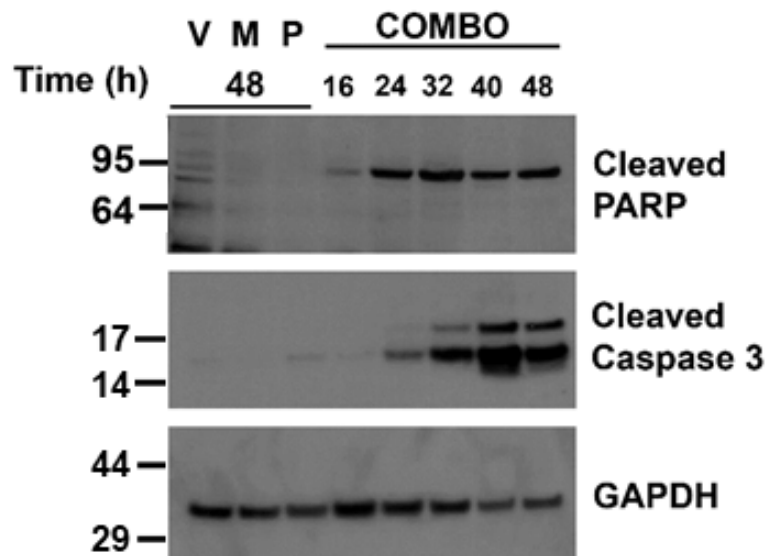
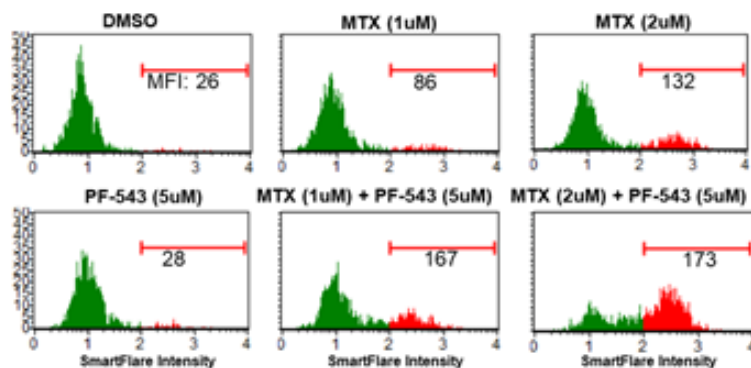
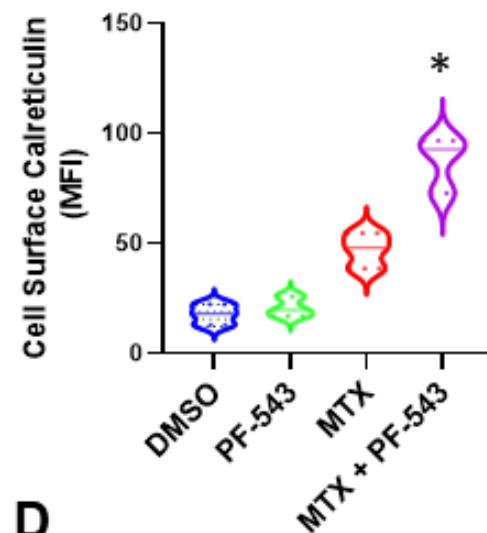


Figure 2

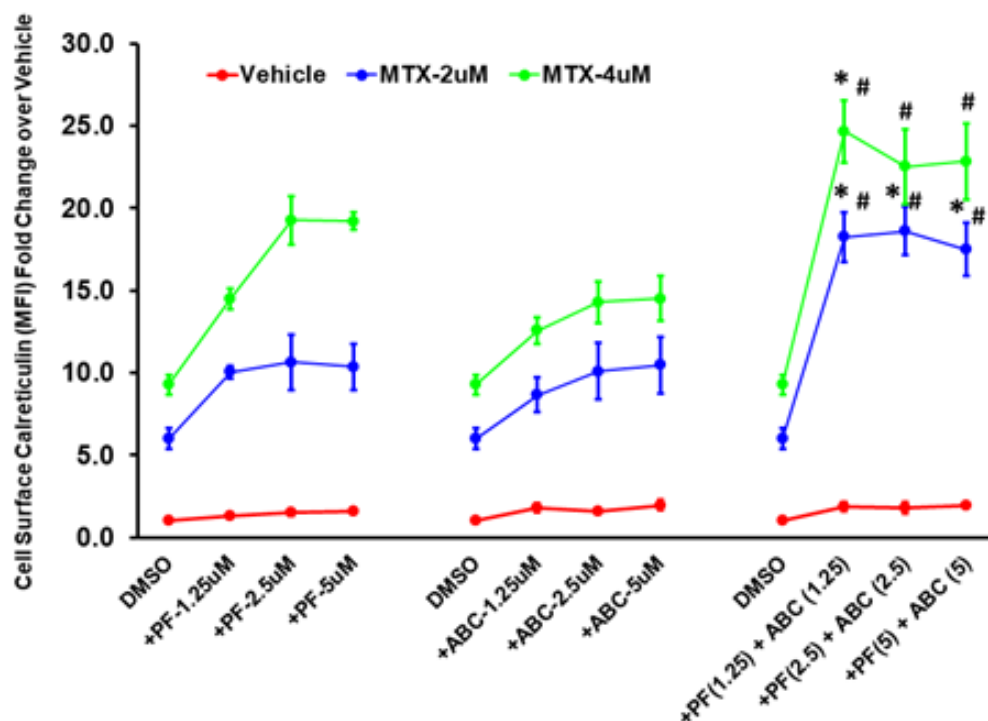
A



B



C



D

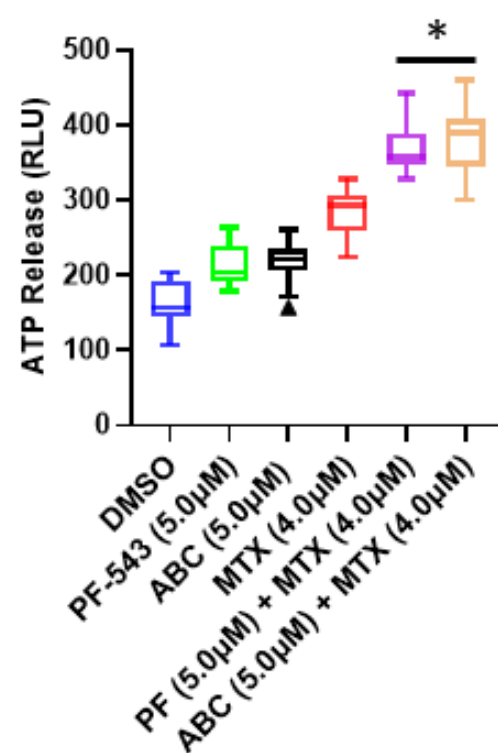
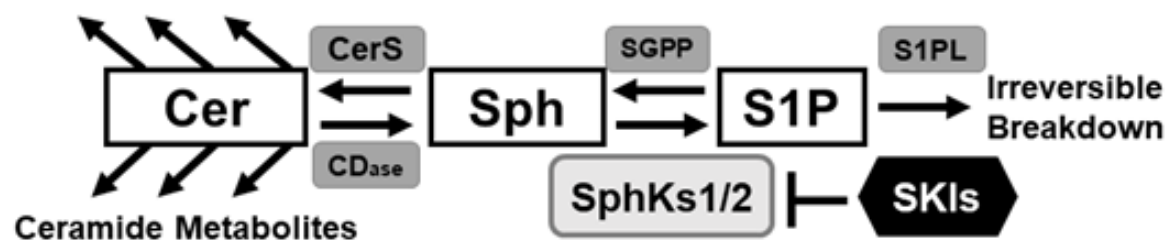


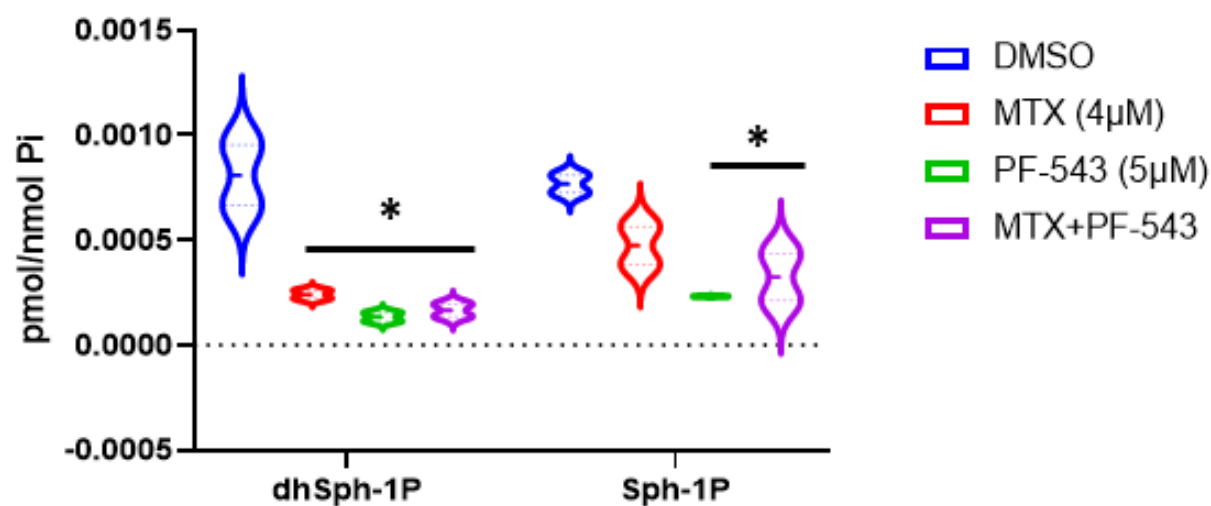
Figure 3

A

Ceramide Metabolites



B



C

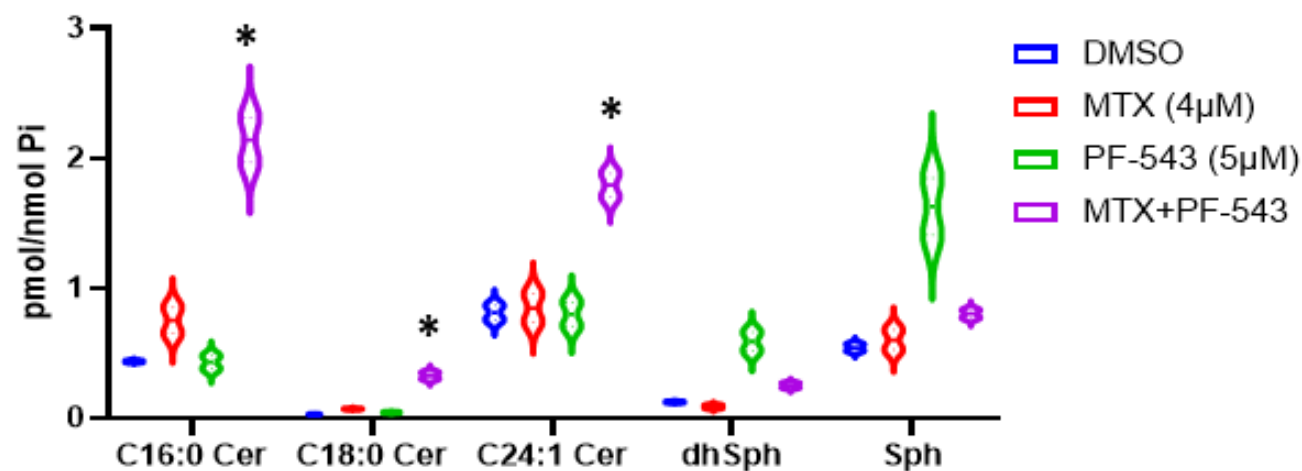
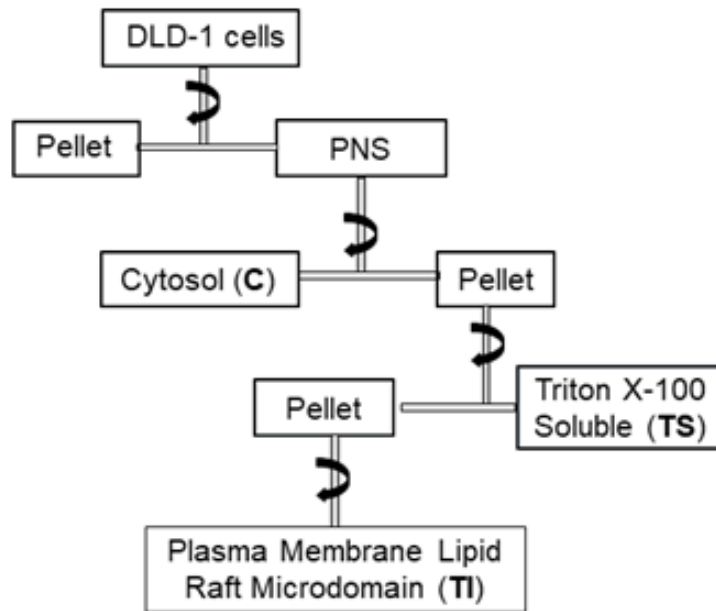


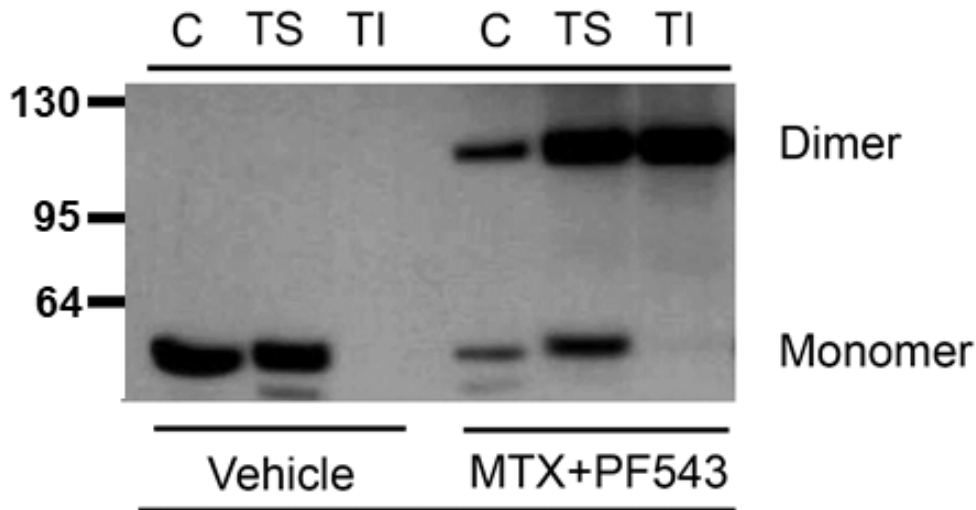
Figure 4



A



B



C

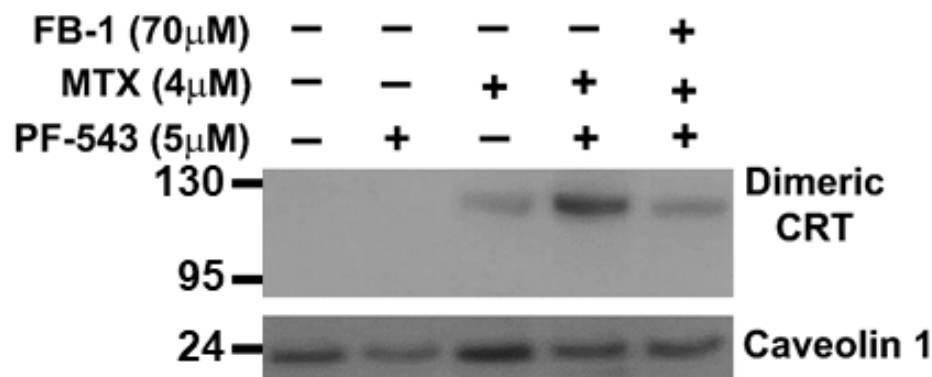


Figure 6